Talanta 233 (2021) 122501

Contents lists available at ScienceDirect

Talanta

journal homepage: www.elsevier.com/locate/talanta

Photosensitive MRI biosensor for BCRP-Targeted uptake and light-induced inhibition of tumor cells

Longhui Zhao [a,b,1], Qianni Guo [a,b,c,1], Chenlu Yuan [a,b], Sha Li [a,b], Yaping Yuan [a,b], Qingbin Zeng [a,b,c], Xu Zhang [a,b], Chaohui Ye [a,b,c], Xin Zhou [a,b,c,*]

[a] Key Laboratory of Magnetic Resonance in Biological Systems, State Key Laboratory of Magnetic Resonance and Atomic and Molecular Physics, National Center for Magnetic Resonance in Wuhan, Wuhan Institute of Physics and Mathematics, Innovation Academy for Precision Measurement Science and Technology, Chinese Academy of Sciences-Wuhan National Laboratory for Optoelectronics, Wuhan, 430071, PR China
[b] University of Chinese Academy of Sciences, Beijing, 100049, PR China
[c] Wuhan National Laboratory for Optoelectronics, Wuhan, 430074, PR China

ARTICLE INFO

Keywords:
Biosensor
Photosensitive MRI
Hyper-CEST

ABSTRACT

Riboflavin and its derivatives are the most important coenzymes in vivo metabolism, and are closely related to life activities. In this paper, the first photolysis ^{129}Xe biosensor was developed by combining cryptophane-A with riboflavin moiety, which showed photosensitivity recorded by hyperpolarized ^{129}Xe NMR/MRI technology with an obvious chemical shift change of 5.3 ppm in aqueous solution. Cellular fluorescence imaging confirmed that the biosensor could be enriched in MCF-7 cells, and MTT assays confirmed that the cytotoxicity was enhanced after irradiation. Findings suggested that the biosensor has a potential application in tumor targeting and the inhibition of tumor cell proliferation after photodegradation.

1. Introduction

Magnetic resonance imaging (MRI) is a valuable medical diagnostic technology, which is non-invasive, non-ionizing radiative, high tissue penetrative, and it has been increasingly used [1]. The traditional MRI is derived from the proton signal of water, and it is difficult to detect samples at physiological concentration because of the lack of sensitivity [2]. Through spin-exchange optical pumping (SEOP) technique, the nuclear spin of the xenon atom can be hyperpolarized and the detection sensitivity can be promoted by more than 100,000-fold compared with the ^{129}Xe of thermal polarization [3]. Besides, ^{129}Xe is very sensitive to environmental changes, and it lacks background noise as a hetero-nucleus, making it an excellent candidate for ultrasensitive biosensors to detect biological target molecules at low concentrations [4]. In 2001, Pines proposed a Xe biosensor format, that is, a functionalized supra-molecular cage (cryptophane-2,2,2 derivative) for hyperpolarized ^{129}Xe (HP ^{129}Xe) encapsulation, which provided distinct encaged ^{129}Xe NMR signals changes for high sensitivity detection of avidins [5]. Great development in HP ^{129}Xe NMR/MRI biosensors has been achieved in the past years [6–11]. Xe biosensors based on supramolecular cages are widely used at present for the detection of molecules/ions [12–16], chemical environment [17,18], and enzyme activities [19–22]. However, no photolysis probe based on HP ^{129}Xe has been developed yet.

Photolysis probes are widely used for photoactivated chemotherapy in specific therapy contexts, such as hypoxic tumors [23]. By applying suitable irradiation, more toxic photolysis byproducts, such as H_2O_2, could be generated to enhance the toxicity of the probes to kill the cells. In neuroscience research [24], they could also regulate protein activity or make protein crosslink through photoproducts. Riboflavin, a water-soluble vitamin [25], could undergo photodegradation, which is classified as an important class of photosensitizers [26,27]. It could be excited to singlet and triplet states, resulting in vast ROS production that causes cell damage and induces apoptosis and intramolecular photo-degradation [28] through suitable irradiation. The photoproducts of riboflavin could also inhibit the growth of tumor cells [29,30]. Riboflavin is a component of two coenzymes, flavin adenine dinucleotide and flavin mononucleotide, which both play important roles in biological redox and energy metabolism [31] Miranda-Lorenzo [32] found that

* Corresponding author. Key Laboratory of Magnetic Resonance in Biological Systems, State Key Laboratory of Magnetic Resonance and Atomic and Molecular Physics, National Center for Magnetic Resonance in Wuhan, Wuhan Institute of Physics and Mathematics, Innovation Academy for Precision Measurement Science and Technology, Chinese Academy of Sciences-Wuhan National Laboratory for Optoelectronics, Wuhan, 430071, PR China.
E-mail address: xinzhou@wipm.ac.cn (X. Zhou).
[1] Longhui Zhao and Qianni Guo These two authors contribute equally to this work.

https://doi.org/10.1016/j.talanta.2021.122501
Received 20 January 2021; Received in revised form 29 April 2021; Accepted 3 May 2021
Available online 17 May 2021

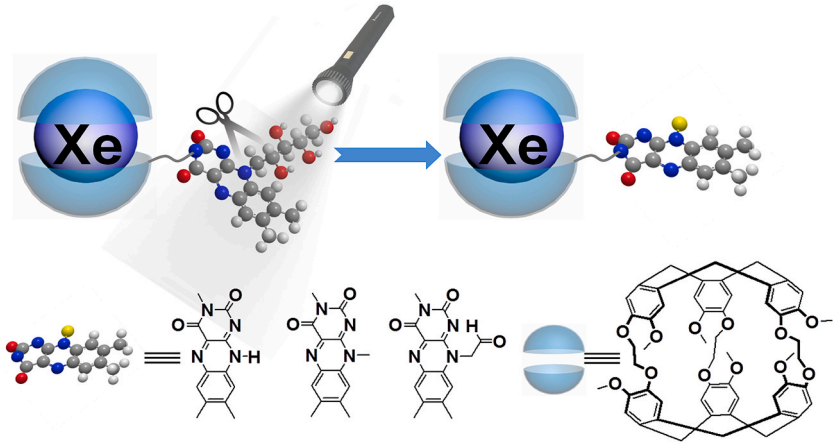

Scheme 1. CrA-2 mechanism of photolysis. Carbon, nitrogen, oxygen, and hydrogen atoms are in gray, red, blue and white, respectively. While the yellow ball refers to the different substituent group, such as –H, $–CH_3$, or $–CH_2CHO$.

riboflavin could be enriched in some tumor cells, such as MCF-7 cells (human breast cancer cells, breast cancer resistance protein/BCRP overexpression). A biosensor modified with riboflavin and its derivatives could be propitious to uptake by tumor cells, which was authenticated in Jabadurai's work [33] thus making biosensor a photosensitizer for the research of cell targeting and tumor cell damage.

In this paper, a novel HP ^{129}Xe biosensor that combined the properties of cryptophane-A and riboflavin was proposed. The design stemmed from the applications of riboflavin and its derivatives as follows. They were potential ligands for tumor targeting. And they also exhibited a certain photochemical response under suitable irradiation to be involved in intramolecular reactions, which could produce photoproducts to enhance the toxicity of the biosensor. In addition, the cryptophane cage acted as a host for the capture of Xe and could serve as the biosensors to monitor the process of reaction via HP ^{129}Xe NMR technology [34]. The present study aimed to establish a biosensor with phototoxicity that could target tumor cells by modifying cryptophane-A with riboflavin derivatives. The prodrug (CrA-1) and the biosensor (CrA-2) synthesis process are shown in Figure S1.

2. Experimental

2.1. Synthesis of riboflavin derivatives

As shown in Scheme 1, CrA-2 was synthesized by riboflavin and cryptophane-A about five steps. The reaction products were characterized by ^{1}H NMR, ^{13}C NMR, and high-resolution mass spectrometry (HRMS; see the Supporting Information). All chemicals and solvents were purchased from the commercial supplier and used without further purification. Room temperature ^{1}H and ^{13}C NMR spectra were recorded in $CDCl_3$ and DMSO-d_6, using a Bruker AMX-500 NMR spectrometer. High-resolution mass spectrometry (HRMS, ESI) spectra were obtained on an Agilent LC/MS QTOF instrument.

2.2. Lamp-house of photolysis

A 250 W high-voltage mercury lamp was used in this work, the emission at 350–450 nm, and the quantum number $N = 1.39 \times 10^{17}\ s^{-1}$ (It was determined by potassium ferrioxalate actinometry).

2.3. Sample preparation

The CrA-2 was dissolved in PBS buffer (pH = 7.4, 20 mM) and 20% DMSO (v/v) to make 50 μM concentration. The solution was illuminated for different time keeping about 25 °C by water bath and then prepared for the measurement of UV–visible/fluorescence or NMR spectrometer. All pH measurements were carried out by Mettler Toledo SevenEasy pH meter. The UV–visible absorption spectra measurements were performed using an Evolution 220 spectrophotometer (Thermofisher Scientific). All solutions and buffers were prepared with distilled water passed through Milli-Q ultrapurification system. Thermo Scientific evolution 220 UV–vis spectrometer, and fluorescence spectra were recorded on an Edinburgh FS5 fluorescence spectrophotometer. The samples for absorption and fluorescence experiments were stored in quartz cuvettes (2 mL volume). The excitation wavelength was 444 nm, and the excitation and emission slit widths were kept at 2 nm.

2.4. ^{129}Xe NMR experiments

Hyperpolarized ^{129}Xe fluid was polarized by the spin-exchange optical pumping method with a home-built polarizer and gas mixture consisting of 10% N_2, and 88% He. 2% Xe (86% enriched ^{129}Xe or natural abundance ^{129}Xe). The hyperpolarized gas mixture was bubbled for 20 s in a 10 mm tailor-made NMR tube containing the solution of interest at the rate of 0.08 standard liters per minute followed by a 3 s delay (to allow bubbles to collapse) prior to signal acquisition. All NMR experiments were conducted on a 9.4 T NMR spectrometer (Bruker Avance 400, Ettlingen, Germany). Unless otherwise stated, The dissolved Xe gas did not escape significantly from the solution during the NMR measurements, as determined by measurements of the partial pressure of the Xe gas, which remained stable. Sample temperature was held 298 K by using a flow of heated N_2 gas. NMR spectra were acquired in PBS buffer (pH = 7.4, containing 20% DMSO-d_6, 10% D_2O). NMR spectra for direct detected were processed using a 10 Hz line broadening filter.

3. Results and discussion

As shown in Scheme 1, considering the photochemical instability of riboflavin ligands in aqueous solution [35], CrA-2 was speculated to have photochemical properties similar to that of riboflavin. As shown in Figure S2, after CrA-2 was exposed to light, its absorbance at 373 and 446 nm obviously decreased. A new absorption peak at 355 nm was generated after applying irradiation. The riboflavin glycosyl chain of CrA-2 was considered to be broken down after photolysis and the chemical structure of CrA-2 to be changed [36]. The 1-hydroxyl of CrA-1 was converted to an acetyloxy group, which made it difficult to accept photoelectrons and generate oxygen free radicals for intramolecular degradation reactions taking place [35,36]. As shown in Figure S2b, the maximum absorption peak of CrA-1 slightly changed after being exposed to long-term irradiation. This result revealed that CrA-2 could provide a theoretical decomposition reaction by applying irradiation but CrA-1

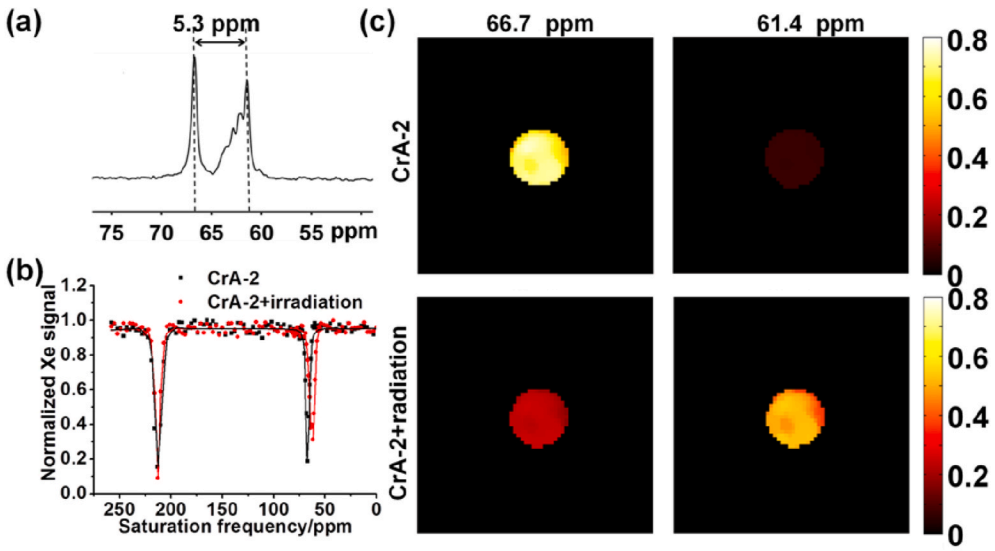

Fig. 1. CrA-2 was used in photolysis after applying irradiation. (a) ^{129}Xe NMR spectra (50 μM, ns = 64) of CrA-2 under 3-h irradiation. (b) Hyper-CEST spectra (12.5 μM) under 4-h irradiation at 10 s of saturation pulse and amplitude of 3.0 μT. The frequency interval from 54 ppm to 84 ppm is 1 ppm, and that of the remaining spectra (0–54, 84–258) is 3 ppm. (c) Hyper-CEST MRI images of a 10 mm tube before and after photolysis of CrA-2. Images were acquired with a saturation pulse excitation centered at δ = 66.7 and 61.4 ppm.

could not proceed because its glycoside chain was protected. The photodissociation dynamics of CrA-2 was also characterized at a narrow pH range of 7.0–8.0, which could affect its ionization states in the solution and susceptibility to excitation [37]. As shown in Figure S2c, the rate of photolysis of CrA-2 followed apparent first-order kinetics and it was the slowest in neutral pH (half-life of 102 min) and then obviously increased (half-life 45 min) in alkaline range. This finding was probably due to the higher reactivity of the flavin triplet in the alkaline range [38]. With the occurrence of photolysis reaction, the concentration of CrA-2 biosensor decreased gradually with fluorescence quenching (Figure S3). These results indicated that CrA-2 was completely photolysed after 3–4 h of irradiation in physiological pH range.

As shown in Figure S4, the ^{129}Xe NMR of CrA-2 was measured, and the results showed encapsulated Xe signal at 66.7 ppm. The HP ^{129}Xe chemical exchange saturation transfer (hyper-CEST) NMR spectrum showed approximately 30% CEST effect when the concentration of CrA-2 was as low as 500 nM. This result implied that the photolysis performance of biosensors could be studied by HP ^{129}Xe NMR technology. After 3 h of irradiation, the spectra exhibited almost the same trend as UV–vis spectra, as shown in Figure S5. The spectral peak of CrA-1 at 72 ppm remained unchanged, while that of CrA-2 remarkably changed. Accurate ^{129}Xe NMR spectral analysis of signals (Fig. 1a) revealed that the original single signal at 66.7 ppm became four main signals located at 66.7, 62.8, 62.0, and 61.4 ppm. These results suggested three main photoproducts, including intermediate products. The possible mechanism was that irradiation caused the gradual breakage of the glycosyl chains on riboflavin moiety, and the electron-withdrawing effect of the original glycosyl chains on the conjugated groups of riboflavin moiety gradually weakened to disappear. As a result, the electron cloud density of the conjugated groups of riboflavin moiety and its influence to the shielding effect of the encapsulated Xe in cryptophane-A cage gradually increased. The increase made the chemical shift of the encapsulated Xe move up-field. The three main photoproducts were collected and analyzed via liquid chromatography–mass spectrometry, as show in Figure S7.

On this basis, the changes in hyper-CEST and MRI before and after photolysis of CrA-2 at pH 7.4 were studied. On the one hand, the chemical shift range from 0 to 258 ppm was selectively saturated and swept, as seen in Fig. 1b, and the hyper-CEST spectra [39] of CrA-2 and its photoproducts were determined. On the other hand, as seen in Fig. 1c, the hyper-CEST MRI images of CrA-2 after 4 h of irradiation were recorded on a 400 MHz Bruker AV400 wide bore spectrometer at saturated resonant frequencies of −145.6 and −150.8 ppm and symmetrical positions of 145.6 and 150.8 ppm (the “cage” Xe signal of CrA-2, the free Xe at 0 ppm) [40]. In virtue of the photochemical reaction of CrA-2, the signal of hyper-CEST changed from 66.7 ppm to 61.4 ppm after photolysis. Analysis of the characteristic of MRI images revealed that the CEST effect at 66.7 ppm before irradiation was 69.3%. It decreased by 72% after complete photolysis. By contrast, the CEST effect at 61.4 ppm increased from 10% to 50%, which realized the transition from “OFF” to

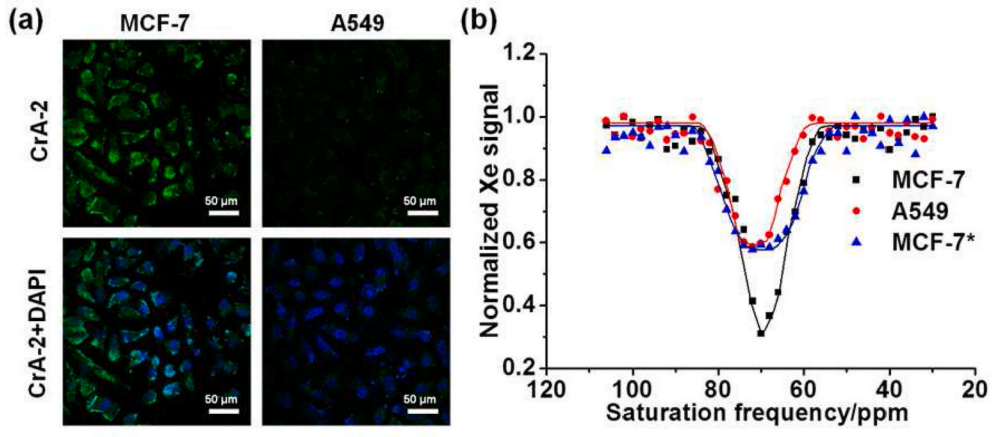

Fig. 2. Uptake of CrA-2 by A549 cells and MCF-7 cells. (a) Fluorescence images of A549 and MCF-7 cells treated by CrA-2 (5 μM) at 37 °C for 3 h. The medium was replaced by fresh medium containing DAPI (0.2 μg/mL), and the cells were incubated for another 5 min; λ_{ex} = 405, 488 nm. (b) Hyper-CEST spectra of CrA-2 (50 μM) in MCF-7 cells (black line) and A549 cells (red line) with its photoproducts in MCF-7 cells (blue line, with the note as MCF-7*). The spectrum was measured with a 10-s saturation pulse and amplitude of 6.5 μT, and the frequency interval from 30 ppm to 106 ppm is 2 ppm. (For interpretation of the references to colour in this figure legend, the reader is referred to the Web version of this article.)

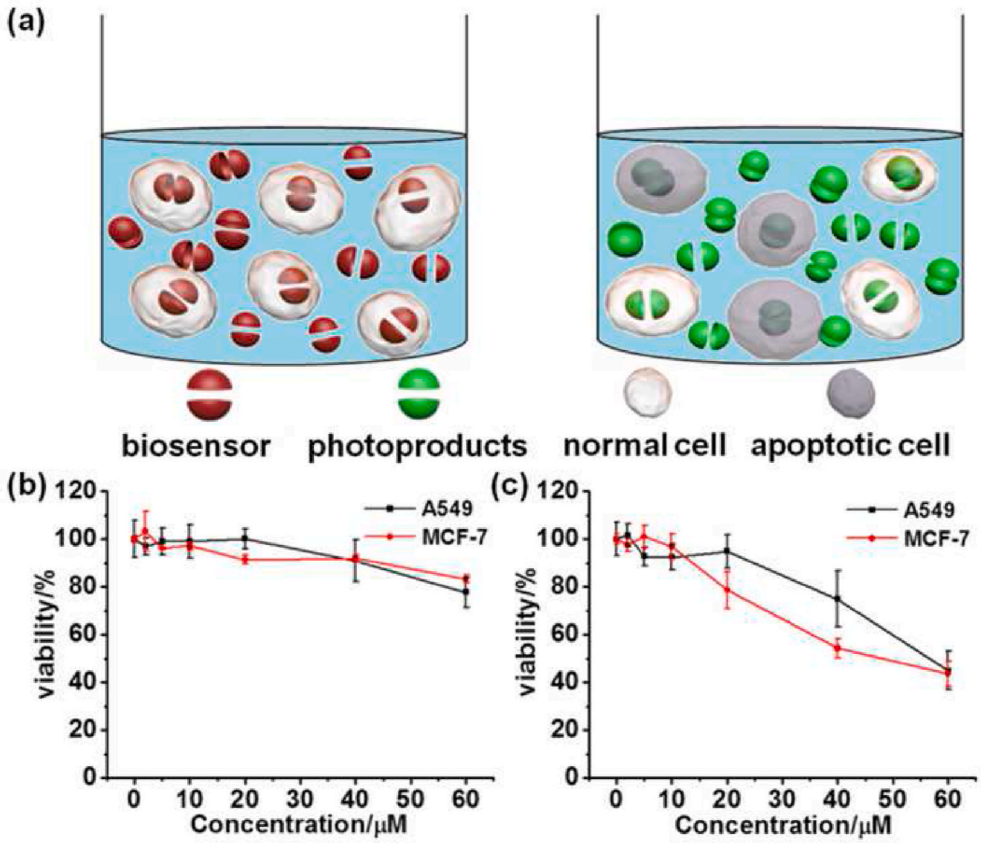

Fig. 3. CrA-2 and its photoproducts were incubated with cells for MTT assay. (a) Photoproducts may be more cytotoxic than CrA-2 in tumor cells. A549 (black line) and MCF-7 (red line) cells after treatment with increasing concentrations of (b) CrA-2 and (c) its photoproducts. Viability was measured using MTT. assay after 24 h of incubation. (For interpretation of the references to colour in this figure legend, the reader is referred to the Web version of this article.)

"ON". These signal changes were also consistent with those in Fig. 1a.

Fluorescence imaging was used to study whether the biosensors could be absorbed by tumor cells. CrA-2 was co-incubated with A549 cells (human lung cancer cells) and MCF-7 cells (BCRP overexpression [41,42]) respectively to investigate whether they could be accumulated by breast cancer resistance protein. In Fig. 2a, at low concentrations, the green fluorescence of MCF-7 cells was much brighter than that of A549 cells. CrA-1/CrA-2 and CrA-1/CrA-2@Elacridar (a BRCP inhibitor) were also incubated with the first two cells. As shown in Figure S8, both went into the cells and showed green fluorescence. In the presence of inhibitors, a remarkable decrease in green fluorescence of biosensors was found in the cells. This result indicated that similar with riboflavin, biosensors, particularly CrA-2, were ingested more effectively by MCF-7. This finding has a positive effect on the study of effective detection of MCF-7 cells.

Hyper-CEST was used to confirm the characteristics of CrA-2 in A549 and MCF-7 cells. The chemical shift of ^{129}Xe NMR range from 32 to 106 ppm was selectively saturated and swept in steps of 2 ppm to test the ^{129}Xe@CrA-2 signal in the cells. As shown in Fig. 2b, in the MCF-7 cells, only one hyper-CEST signal appeared at approximately 68 ppm, which corresponded to ^{129}Xe@CrA-2, whereas a similar weakened signal was found in A549 cells. This result was consistent with the data of fluorescence images, indicating that CrA-2 could be better accumulated by MCF-7 cells than A549 cells. This finding also showed its targeting due to the overexpression of breast cancer resistance protein in the MCF-7 cells. Therefore, MCF-7 cells were selected for further detection to confirm whether the change of biosensors after photolysis could be probed in the cells by ^{129}Xe hyper-CEST. After irradiation was conducted, the intensity of the CEST signal of CrA-2 attenuated by approximately 40%, whereas that of CrA-1 demonstrated a slight change (Figure S9), and the signal width significantly widened. This result indicated that because of the complex intracellular environment [17,18,43], the CrA-2 and photoproducts could not be accurately distinguished by the chemical shifts. However, the photodegradation of CrA-2 in MCF-7 cells could still be investigated depending on the change in intensity and width of the ^{129}Xe hyper-CEST signal.

In addition, the cytotoxicity of CrA-1/CrA-2 and their photoproducts to A549 and MCF-7 cells were determined by MTT assay. As shown in Figure S10, after the CrA-1 incubated with MCF-7, the cells viability was only approximately 60% at 60 μM, after the photoproducts of CrA-1 incubated with cells, the cells viability almost had not any change. On the contrary, before irradiation, when the concentration of CrA-2 was not more than 40 μM, the viability of both cells remained above 90%, as shown in Fig. 3b. When the concentration of CrA-2 reached 60 μM, the viability of both cells decreased slightly to around 80% but still maintained a high level. This finding indicated that CrA-2 had lower cytotoxicity than CrA-1. As shown in Fig. 3c, the photoproducts of CrA-2 was incubated with A549 and MCF-7 cells. When the concentration of photoproducts was less than 10 μM, the viability of MCF-7 cells was kept in good condition. But the tolerance of MCF-7 cells suddenly dropped when the concentration was increased from 10 μM to 60 μM, and the viability was only 40% after 24 h of incubation at 60 μM concentration. And resembling phenomena was observed in A549 cells (balck line). Results suggested that the photoproducts of CrA-2 were able to inhibit the viability of A549 and MCF-7 cells, especially MCF-7 cells. Most photosensitizers were reported to focus on supplying singlet oxygen after short-term irradiation to inhibit the activity of tumor cells, in which riboflavin and its derivatives were utilized [44]. Only few studies on the effect of photoproducts on tumor cells were carried out [29,30]. The photoproducts of riboflavin and its derivatives could also inhibit tumor

cell proliferation. Therefore, CrA-2 has a potential to be a photosensitive drug that could target MCF-7 cells and inhibit them by applying appropriate irradiation.

4. Conclusion

In summary, a new photosensitive biosensor was developed. It could target MCF-7 cells specifically compared with A549 cells by intracellular hyper-CEST experiments and fluorescence imaging. The MTT assay showed MCF-7 cells had more than 80% cell viability when incubated with CrA-2 at 60 μM for 24 h. When incubated MCF-7 cells with the photoproducts in the same condition, significant inhibition of cell activity can be observed. The results above indicated that the CrA-2 can target MCF-7 cells and inhibit tumor cells proliferation after photodegradation. It has potential to be applied as a photosensitizers for targeting inhibition of tumor cells.

Author contributions

Longhui Zhao; Compound synthesis, formal analysis, data curation, writing original draft. Qianni Guo; conceptualization, methodology, resources, supervision, project administration, funding acquisition, validation, writing review and editing. Chenlu Yuan; Validation, formal analysis, compound synthesis, Sha Li; Investigation, validation, formal analysis. Yaping Yuan; Validation, formal analysis. Qingbin Zeng; writing review and editing. Xu Zhang; Validation, formal analysis. Chaohui Ye; Resources, funding acquisition. Xin Zhou[1]; resources, supervision, project administration, funding acquisition, validation, writing review and editing.

Zhao and Guo contributed equally to this work.

Declaration of competing interest

The authors declare that they have no known competing financial interests or personal relationships that could have appeared to influence the work reported in this paper.

Acknowledgements

This work is supported by National Key R&D Program of China (2018YFA0704000, 2016YFC1304700), and National Natural Science Foundation of China (81625011, 91859206, 81730048, 81971705).

Appendix A. Supplementary data

Supplementary data to this article can be found online at https://doi.org/10.1016/j.talanta.2021.122501.

References

[1] E. Terreno, D.D. Castelli, A. Viale, S. Aime, Challenges for molecular magnetic resonance imaging, Chem. Rev. 110 (2010) 3019–3042.
[2] Z. Xu, C. Liu, S. Zhao, S. Chen, Y. Zhao, Molecular sensors for NMR-based detection, Chem. Rev. 119 (2019) 195–230.
[3] Q. Zeng, B. Bie, Q. Guo, Y. Yuan, Q. Han, X. Han, M. Cheng, X. Zhang, Y. Yang, M. Liu, H. Deng, X. Zhou, Hyperpolarized Xe NMR signal advancement by metal-organic framework entrapment in aqueous solution, Proc. Natl. Acad. Sci. U.S.A. 117 (2020) 17558–17563.
[4] K.W. Miller, N.V. Reo, A. Uiterkamp, D. Stengle, T.R. Stengle, K.L. Williamson, Xenon NMR: chemical shifts of a general anesthetic in common solvents, proteins, and membranes, Proc. Natl. Acad. Sci. U.S.A. 78 (1981) 4946–4949.
[5] M.M. Spence, S.M. Rubin, I.E. Dimitrov, E.J. Ruiz, D.E. Wemmer, A. Pines, S. Q. Yao, F. Tian, P.G. Schultz A, Directly functionalized cucurbit[7]uril as a biosensor for the selective detection of protein interactions by Xe-129 hyperCEST NMR, Proc. Natl. Acad. Sci. U.S.A. 98 (2001) 10654–10657.
[6] N. Kotera, E. Dubost, G. Milanole, E. Doris, E. Gravel, N. Arhel, T. Brotin, J.-P. Dutasta, J. Cochrane, E. Mari, C. Boutin, E. Leonce, P. Berthault, B. Rousseau, A doubly responsive probe for the detection of Cys4-tagged proteins, Chem. Commun. 51 (2015) 11482–11484.
[7] E. Dubost, J.P. Dognon, B. Rousseau, G. Milanole, C. Dugave, Y. Boulard, E. Leonce, C. Boutin, P. Berthault, Understanding a host-guest model system through Xe-129 NMR spectroscopic experiments and theoretical studies, Angew. Chem. Int. Ed. 53 (2014) 9837–9840.
[8] Q. Zeng, Q. Guo, Y. Yuan, Y. Yang, B. Zhang, L. Ren, X. Zhang, Q. Luo, M. Liu, L. S. Bouchard, X. Zhou, Mitochondria targeted and intracellular biothiol triggered hyperpolarized ^{129}Xe magnetofluorescent biosensor, Anal. Chem. 89 (2017) 2288–2295.
[9] Y. Wang, B.W. Roose, J.P. Philbin, J.L. Doman, I.J. Dmochowski, Programming a molecular relay for ultrasensitive biodetection through Xe-129 NMR, Angew. Chem. Int. Ed. 55 (2016) 1733–1736.
[10] M. Kunth, G. Lu, C. Witte, M.G. Shapiro, L. Schroder, Protein nanostructures produce self-adjusting hyperpolarized magnetic resonance imaging contrast through physical gas partitioning, ACS Nano 12 (2018) 10939–10948.
[11] S.H. Klass, A.E. Truxal, T.A. Fiala, J. Kelly, D. Nguyen, J.A. Finbloom, D. E. Wemmer, A. Pines, M.B. Francis, Rotaxane probes for the detection of hydrogen peroxide by ^{129}Xe HyperCEST NMR spectroscopy, Angew. Chem. Int. Ed. 58 (2019) 9948–9953.
[12] A. Schlundt, W. Kilian, M. Beyermann, J. Sticht, S. Gunther, S. Hopner, K. Falk, O. Roetzschke, L. Mitschang, C. Freund, Multichannel MRI labeling of mammalian cells by switchable nanocarriers for hyperpolarized xenon, Angew. Chem. Int. Ed. 48 (2009) 4142–4145.
[13] S. Yang, W. Jiang, L. Ren, Y. Yuan, B. Zhang, Q. Luo, Q. Guo, L.S. Bouchard, M. Liu, X. Zhou, Biothiol xenon MRI sensor based on thiol-addition reaction, Anal. Chem. 88 (2016) 5835–5840.
[14] S. Yang, Y. Yuan, W. Jiang, L. Ren, H. Deng, L.S. Bouchard, X. Zhou, M. Liu, Hyperpolarized ^{129}Xe MRI sensor for H_2S, Chem. Eur J. 23 (2017) 7648–7652.
[15] D. Zhang, T.K. Ronson, J.L. Greenfield, T. Brotin, P. Berthault, E. Leonce, J.L. Zhu, L. Xu, J.R. Nitschke, Enantiopure [Cs^+/Xe subset of cryptophane]subset of(Fe_4L_4)-L-II hierarchical superstructures, J. Am. Chem. Soc. 141 (2019) 8339–8345.
[16] Q. Guo, Q. Zeng, W. Jiang, X. Zhang, Q. Luo, X. Zhang, L.S. Bouchard, M. Liu, X. Zhou, A molecular imaging approach to mercury sensing based on hyperpolarized ^{129}Xe molecular clamp probe, Chem. Eur J. 22 (2016) 3967–3970.
[17] B.A. Riggle, Y. Wang, I.J. Dmochowski, A "smart" Xe-129 NMR biosensor for pH-dependent cell labeling, J. Am. Chem. Soc. 137 (2015) 5542–5548.
[18] E. Leonce, J.P. Dognon, D. Pitrat, J.C. Mulatier, T. Brotin, P. Berthault, Accurate pH sensing using hyperpolarized Xe-129 NMR spectroscopy, Chem. Eur J. 24 (2018) 6534–6537.
[19] J.M. Chambers, P.A. Hill, J.A. Aaron, Z.H. Han, D.W. Christianson, N.N. Kuzma, I. J. Dmochowski, Cryptophane xenon-129 nuclear magnetic resonance biosensors targeting human carbonic anhydrase, J. Am. Chem. Soc. 131 (2009) 563–569.
[20] S. Klippel, J. Dopfert, J. Jayapaul, M. Kunth, F. Rossella, M. Schnurr, C. Witte, C. Freund, L. Schroder, Supramolecular assays for mapping enzyme activity by displacement-triggered change in hyperpolarized Xe-129 magnetization transfer NMR spectroscopy, Angew. Chem. Int. Ed. 54 (2015) 13444–13447.
[21] J.A. Finbloom, C.C. Slack, C.J. Bruns, K. Jeong, D.E. Wemmer, A. Pines, M. B. Francis, Rotaxane-mediated suppression and activation of cucurbit[6]uril for molecular detection by Xe-129 hyperCEST NMR, Chem. Commun. 52 (2016) 3119–3122.
[22] B. Zhang, Q. Guo, Q. Luo, X. Zhang, Q. Zeng, L. Zhao, Y. Yuan, W. Jiang, Y. Yang, M. Liu, C. Ye, X. Zhou, An intracellular diamine oxidase triggered hyperpolarized ^{129}Xe magnetic resonance biosensor, Chem. Commun. 54 (2018) 13654–13657.
[23] M. Li, N.K. Wong, J. Xiao, R. Zhu, L. Wu, S. Dai, G. Huang, L. Xu, X. Bai, M. R. Geraskina, A.H. Winter, X. Chen, Y. Liu, W. Fang, D. Yang, D.L. Phillips, Dynamics of oxygen-independent photocleavage of blebbistatin as a one-photon blue or two-photon near-infrared light-gated hydroxyl radical photocage, J. Am. Chem. Soc. 140 (2018) 15957–15968.
[24] M.T. Richers, J.M. Amatrudo, J.P. Olson, G.C.R. Ellis-Davies, Cloaked caged compounds: chemical probes for two-photon optoneurobiology, Angew. Chem. Int. Ed. 56 (2017) 193–197.
[25] C.W. Mason, V.M. D'Souza, L.M. Bareford, M.A. Phelps, A. Ray, W. Swaan, Recognition, co-internalization, and recycling of an avian riboflavin carrier protein in human placental trophoblast, J. Pharmacol. Exp. Therapeut. 317 (2006) 465–472.
[26] Y. Bi, Z. Huang, B. Liu, Q. Zou, J. Yu, Y. Zhao, Q. Luo, Two-photon-excited fluorescence and two-photon spectrofluoroelectrochemistry of riboflavin, Electrochem. Commun. 4 (2006) 595–599.
[27] J. Liang, M. Yuan, C. Cheng, H. Jian, C. Lin, Y. Chen, Blue light induced free radicals from riboflavin on E. coli DNA damage, Photochem. Photobiol. B. 119 (2013) 60–64.
[28] M.A. Sheraz, S.H. Kazi, S. Ahmed, Z. Anwar, I. Ahmad, A possible anti-proliferative and anti-metastatic effect of irradiated riboflavin in solid tumours, Beilstein J. Org. Chem. 10 (2014) 1999–2012.
[29] K.C.D. Queiroz, W.F. Zambuzzi, A.C.S. de Souza, R.A. da Silva, D. Machado, G. Z. Justo, H.F. Carvalho, M.P. Peppelenbosch, C.V. Ferreira, A possible anti-proliferative and anti-metastatic effect of irradiated riboflavin in solid tumours, Canc. Lett. 258 (2007) 126–134.
[30] A.C. De Souza, L. Kodach, F.R. Gadelha, C.L. Bos, A.D. Cavagis, H. Aoyama, M.P. M Peppelenbosch, C.V. Ferreira, A promising action of riboflavin as a mediator of leukaemia cell death, Apoptosis 11 (2006) 1761–1771.
[31] A. Orita, M.G. Verde, M. Sakai, Y.S. Meng, A biomimetic redox flow battery based on flavin mononucleotide, Nat. Commun. 7 (2016) 13230.
[32] I. Miranda-Lorenzo, J. Dorado, E. Lonardo, S. Alcala, A.G. Serrano, J. Clausell-Tormos, M. Cioffi, D. Megias, S. Zagorac, A. Balic, M. Hidalgo, M. Erkan, J. Kleeff, A. Scarpa, B. Sainz, C. Heeschen, Intracellular autofluorescence: a biomarker for epithelial cancer stem cells, Nat. Methods 11 (2014) 1161–1169.
[33] J. Jayapaul, M. Hodenius, S. Arns, W. Lederle, T. Lammers, P. Comba, F. Kiessling, J. Gaetjens, FMN-coated fluorescent iron oxide nanoparticles for RCP-mediated

targeting and labeling of metabolically active cancer and endothelial cells, Biomaterials 32 (2011) 5863–5871.
[34] R. Tyagi, C. Witte, R. Haag, L. Schroder, Dendronized cryptophanes as water-soluble xenon hosts for ^{129}Xe magnetic resonance imaging, Org. Lett. 16 (2014) 4436–4439.
[35] M.I. Gutierrez, S.M. Fernandez, W.A. Massad, N.A. Garcia, Kinetic study on the photostability of riboflavin in the presence of barbituric acid, Redox Rep. 11 (2006) 1743–2928.
[36] I. Ahmad, S. Ahmed, M.A. Sheraz, M. Aminuddin, F.H.M. Vaid, Effect of complexation on the photolysis of riboflavin in aqueous solution: a kinetic study, Chem. Pharm. Bull. 57 (2009) 1363–1370.
[37] I. Ahmad, S. Ahmed, M.A. Sheraz, F.H.M. Vaid, Effect of borate buffer on the photolysis of riboflavin in aqueous solution, J. Photochem. Photobiol., B 93 (2008) 82–87.
[38] I. Ahmad, Q. Fasihullah, A. Noor, I.A. Ansari, Q.N.M. Ali, Photolysis of riboflavin in aqueous solution: a kinetic study, Int. J. Pharm. 280 (2004) 199–208.
[39] Y. Bai, P.A. Hill, I.J. Dmochowski, Utilizing a water-soluble cryptophane with fast xenon exchange rates for picomolar sensitivity NMR measurements, Anal. Chem. 84 (2012) 9935–9941.
[40] F.T. Hane, T. Li, P. Smylie, R.M. Pellizzari, J.A. Plata, B. DeBoef, M.S. Albert, In vivo detection of cucurbit[6]uril, a hyperpolarized xenon contrast agent for a xenon magnetic resonance imaging biosensor, Sci. Rep. 7 (2017) 41027.
[41] I. Ifergan, G.L. Scheffer, Y.G. Assaraf, Riboflavin concentration within ABCG2-rich extracellular vesicles is a novel marker for multidrug resistance in malignant cells, Canc. Res. 65 (2005) 10952–10958.
[42] M. Zhang, W. Wang, N. Zhou, P. Yuan, Y. Su, M. Shao, C. Chi, F. Pan, Near-infrared light triggered photo-therapy, in combination with chemotherapy using magnetofluorescent carbon quantum dots for effective cancer treating, Carbon 118 (2017) 752–764.
[43] S. Klippel, J. Dopfert, J. Jayapaul, M. Kunth, F. Rossella, M. Schnurr, C. Witte, C. Freund, L. Schroder, Cell tracking with caged xenon: using cryptophanes as MRI reporters upon cellular internalization, Angew. Chem. Int. Ed. 53 (2014) 493–496.
[44] M.Y. Yang, C.J. Chang, L.Y. Chen, Blue light induced reactive oxygen species from flavin mononucleotide and flavin adenine dinucleotide on lethality of HeLa cells Photoch, Photobio. B. 173 (2017) 325–332.